Magnetostructural studies of copper(II)–verdazyl radical complexes†‡

Joe B. Gilroy,[a] Bryan D. Koivisto,[a] Robert McDonald,[b] Michael J. Ferguson[b] and Robin G. Hicks*[a]

Received 10th March 2006, Accepted 4th May 2006
First published as an Advance Article on the web 16th May 2006
DOI: 10.1039/b603624d

The synthesis, structures, and magnetic properties of several Cu(II) complexes of verdazyl radicals are presented. Reactions of chelating verdazyl radicals with either $CuCl_2 \cdot 2H_2O$ or $Cu(hfac)_2 \cdot 2H_2O$ produced 1 : 1 Cu : verdazyl complexes with either chloride or hfac ancillary ligands. Structural characterization reveals that the $CuCl_2$ complexes of *N*,*N*′-dimethyl-3-(2-pyridyl)-6-oxoverdazyl or *N*,*N*′-bis(isopropyl)-3-(2-pyridyl)-6-oxoverdazyl have pseudo-square pyramidal copper ions with verdazyl rings bound in equatorial positions, while the $Cu(hfac)_2$ complex of *N*,*N*′-dimethyl-3-(*N*-methyl-2-imidazolyl)-6-oxoverdazyl is Jahn–Teller distorted pseudo-octahedral and has the verdazyl nitrogen axially bound. Variable temperature magnetic susceptibility studies reveal that equatorially bound verdazyls are strongly antiferromagnetically coupled, while the axially bound radicals are weakly ferromagnetically coupled. Intermolecular magnetic interactions are also an important component of the overall magnetism in these systems.

Introduction

The ''metal–radical'' approach[1] is one of the more attractive strategies for the design of molecule-based materials with magnetic ordering temperatures (T_Cs) near ambient. The ideal structure of a metal–radical magnet is a multidimensional coordination network consisting of paramagnetic metal ions linked by bridging, *paramagnetic* ligands (radicals) in which metal and ligand based spins are engaged in sufficiently strong exchange interactions to support long range magnetic order. Metal–radical magnets based on cyanocarbon radical anions[2] or nitroxide radicals[3] highlight the potential of the metal–radical approach, but both classes of materials suffer from limitations (low T_C in the case of nitroxides; lack of structural information and/or air instability for the radical anions) which have in part motivated explorations of new kinds of paramagnetic ligands.

Recent work by us[4] and others[5,6] has demonstrated that verdazyl radicals **1** are effective ligands for transition metal complexes. In all cases the verdazyls are judiciously substituted to create chelating binding sites (*e.g.* the 2-pyridyl substituted verdazyl **2**). In complexes of paramagnetic metal ions, the verdazyl–metal magnetic exchange is found to be metal-dependent: Mn(II)–verdazyl exchange is moderate and antiferromagnetic, whereas Ni(II) complexes exhibit ferromagnetic coupling, in some instances quite strongly so. As part of our efforts to further develop verdazyl coordination chemistry as a new set of building blocks for metal–radical-based magnets, we became interested in the corresponding Cu(II) complexes. Only one such complex has been reported,[4f] though Cu(I) complexes are known.[5] Herein we describe the synthesis, structures and magnetochemistry of several Cu(II) complexes of verdazyl-based ligands **2–4**.

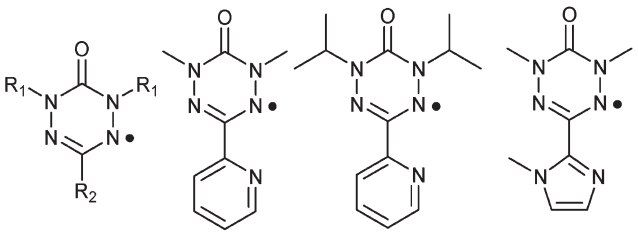

1 **2** **3** **4**

Experimental

General considerations

All reactions and manipulations were carried out under an argon atmosphere using standard Schlenk or glovebox techniques. All reagents were purchased from Aldrich and used as received. Verdazyl radicals **2**[7] and **3**[8] and $Cu(hfac)_2 \cdot 2H_2O$[9] were prepared according to literature procedures. Elemental analyses were carried out by Canadian Microanalytical Services Ltd., Vancouver, BC. NMR spectra were recorded on a Bruker AMX300 spectrometer. EPR spectra were recorded on a Bruker EMX300 instrument. Mass spectra were recorded on a Kratos Concept IH mass spectrometer system. UV-Vis spectra were recorded using a Cary 50 Scan instrument. IR spectra were recorded as KBr presses on a Perkin Elmer Spectrum One Spectrometer.

1,5-Dimethyl-3-(1-methyl-2-imidazolyl)-1,2,4,5-tetrazane-6-oxide (5). A solution of *N*-methyl-2-imidazole carboxaldehyde (2.0 g, 18.2 mmol) in 200 mL of methanol was added dropwise to a refluxing solution of carbonic acid bis(methylhydrazide)[7]

[a]*Department of Chemistry, University of Victoria, PO Box 3065 STN CSC, Victoria, BC, V8W 3V6, Canada. E-mail: rhicks@uvic.ca*
[b]*X-Ray Crystallography Laboratory, Department of Chemistry, University of Alberta, Edmonton, Alberta, T6G 2G2, Canada*
† This article is part of a themed issue on Molecular Magnetic Materials.
‡ Electronic supplementary information (ESI) available: compound characterization details and spectra. See DOI: 10.1039/b603624d

(2.146 g, 18.2 mmol) in 10 mL of methanol. The mixture was refluxed for 10 h and the solvent was then removed under vacuum. Pure samples of **5** were obtained *via* repeated trituration with ethyl acetate. Washings were treated with ether to recover **5** as a colourless microcrystalline solid, yield 2.96 g (77.5%). Mp 176 °C (decomp.). ^{1}H NMR (d_6-DMSO): δ 7.14 (s, 1H), 6.83 (s, 1H), 5.58 (d, 2H, J = 11Hz), 5.07 (t, 1H, J = 11Hz), 3.68 (s, 3H), 2.95 (s, 6H) ppm. ^{13}C NMR ($CDCl_3$): δ 154.6, 141.7, 128.0, 122.3, 63.0, 38.1, 32.9 ppm. FT-IR (KBr): ν(CO) 1633 (s) cm^{-1}. MS (EI): m/z 210 {M^+, 50%}. HR-MS: 210.1227 $\pm$ 0.0002 (210.1229 for $M^+C_8H_{14}N_6O$). Anal. Calcd for $C_8H_{14}N_6O$: C, 45.70; H, 6.71; N, 39.97. Found: C, 45.75; H, 6.74; N, 40.41%.

1,5-Dimethyl-3-(1-methyl-2-imidazolyl)-6-oxoverdazyl (4). A solution of sodium periodate (0.229 g, 1.07 mmol) in 10 mL of distilled water was added to a vigorously stirred slurry of **5** (0.15 g, 0.71 mmol) in 20 mL of distilled water resulting in a cherry red solution. After 10 min of stirring the solution was placed in an ice bath for 30 min resulting in the precipitation of **4** as a microcrystalline red solid, yield 0.103 g (68%). Mp 165 °C (decomp.). FT-IR (KBr): ν(CO) 1674 (s) cm^{-1}. UV-Vis (CH_2Cl_2): λ_{max} 415 nm (ε = 1100), 493 nm (ε = 410). MS (LSIMS): m/z 207 {MH^+, 100%}, 107 {80%}. HR-MS: 207.0991 $\pm$ 0.0003 (207.0994 for $MH^+C_8H_{12}N_6O$). Anal. Calcd for $C_8H_{11}N_6O$: C, 46.37; H, 5.35; N, 40.56. Found: C, 46.20; H, 5.38; N, 40.68%.

Cu(2)Cl$_2$ (6). A solution of **2** (freshly separated from hydroquinone by flash chromatography; 0.072 g, 0.35 mmol) in 2 mL of ethanol was added to a solution of $CuCl_2{\cdot}2H_2O$ (0.060 g, 0.35 mmol) in 2 mL ethanol. The solution immediately turned dark red. After 5 min of gentle heating the solution was cooled to −15 °C overnight resulting in the precipitation of **6** as a dark red crystalline solid, yield 0.095 g (80%). Single crystals were grown by solvent diffusion of hexane into a dichloromethane solution of **6**. Mp 102–104 °C (decomp.). FT-IR (KBr): ν(CO) 1697 (s) cm^{-1}. UV-Vis (CH_2Cl_2): λ_{max} 280 nm (ε = 7500), 492 nm (ε = 3750). Anal. Calcd for $C_9H_{10}N_5OCuCl_2$: C, 31.92; H, 2.98; N, 20.68. Found: C, 32.05; H, 3.13; N, 19.95%.

[Cu(3)Cl$_2$]$_2$ (7). A solution of **3** (0.050 g, 0.19 mmol) in 2 mL of ethanol was added to a solution of $CuCl_2{\cdot}2H_2O$ (0.032 g, 0.19 mmol) in 1 mL of ethanol. The solution immediately turned red–purple, and after 5 min of gentle heating was cooled to −15 °C overnight resulting in the precipitation of **7** as a dark red crystalline solid, yield 0.054 g (72%). Single crystals were grown by slow evaporation of a saturated 1 : 1 solution of **7** in dichloromethane and hexane. Mp 112–114 °C (decomp.). FT-IR (KBr): ν(CO) 1702 (s) cm^{-1}. UV-Vis (CH_2Cl_2): λ_{max} 281 nm (ε = 12750), 500 nm (ε = 5750). Anal. Calcd for $C_{13}H_{18}N_5OCuCl_2$: C, 39.55; H, 4.60; N, 17.74. Found: C, 39.54; H, 4.61; N, 17.87%.

Cu(2)(hfac)$_2$ (8). A solution of **2** : hydroquinone (0.216 g, 0.68 mmol) in 10 mL dichloromethane was added to a slurry of $Cu(hfac)_2{\cdot}2H_2O$ (0.328 g, 0.64 mmol) in 30 mL heptane. The solution immediately turned light brown, and after 30 min a white precipitate formed. The solution was filtered and the filtrate solvent was removed *in vacuo* leaving a microcrystalline brown solid. Recrystallization from hexanes yielded **8** as gold needles, yield 0.330 g (76%). Mp 94–97 °C (decomp.). FT-IR (KBr): ν(CO) 1705 (s) cm^{-1}. UV-Vis (CH_2Cl_2): λ_{max} 421 nm (ε = 2800). Anal. Calcd for $C_{19}H_{12}N_5O_5F_{12}Cu$: C, 33.47; H, 1.77; N, 10.27. Found: C, 33.60; H, 1.60; N, 10.59%.

Cu(4)(hfac)$_2$ (9). A solution of **4** (0.090 g, 0.44 mmol) in 10 mL dichloromethane was added to a slurry of $Cu(hfac)_2{\cdot}2H_2O$ (0.224 g, 0.44 mmol) in 20 mL heptane. The solution immediately turned pink, and upon refluxing for 1 h became dark red. The solvent was removed *in vacuo* leaving a microcrystalline red solid. Recrystallization from ethanol afforded **9** as single crystals, yield 0.195 g (65%). Mp 86–88 °C (decomp.). FT-IR (KBr): ν(CO) 1712 (s) cm^{-1}. UV-Vis (CH_2Cl_2): λ_{max} 422 nm (ε = 3100). Anal. Calcd for $C_{18}H_{13}N_6O_5F_{12}Cu$: C, 31.57; H, 1.91; N, 12.27. Found: C, 31.53; H, 2.03; N, 12.27%.

X-Ray structure determination

X-Ray diffraction data (Table 1) were collected on a Bruker PLATFORM/SMART 1000 CCD with

Table 1 Crystallographic data

	3	**6**	**7**	**9**
Formula	$C_{13}H_{18}N_5O$	$C_9H_{10}Cl_2CuN_5O$	$C_{13}H_{18}Cl_2CuN_5O$	$C_{18}H_{13}CuF_{12}N_6O_5$
FW	260.32	338.66	394.76	684.88
a/Å	5.1997(13)	14.9568(12)	12.2769(13)	9.8110(9)
b/Å	26.382(7)	9.9809(8)	10.7994(8)	10.9073(10)
c/Å	10.429(3)	17.3231(14)	17.8486(14)	12.5202(12)
α/°	90	90	90	78.5653(14)
β/°	103.785(4)	90	90	83.4385(14)
γ/°	90	90	90	73.699(14)
Volume/Å^3	1394.7(6)	2586.0(4)	3330.2(4)	1258.0(2)
Space group	$P2_1/c$	$Pbca$	$Pbca$	$P\bar{1}$
Z	4	8	8	2
μ(Mo-Kα)/mm^{-1}	0.084	2.096	1.640	1.000
T/K	193.15	193.15	193.15	273.15
Independent reflections	2853	2639	3417	5142
	R_{int} = 0.0706	R_{int} = 0.0220	R_{int} = 0.0202	R_{int} = 0.0305
R	0.0524	0.0230	0.0488	0.0453
wR	0.1187	0.0656	0.1137	0.1302

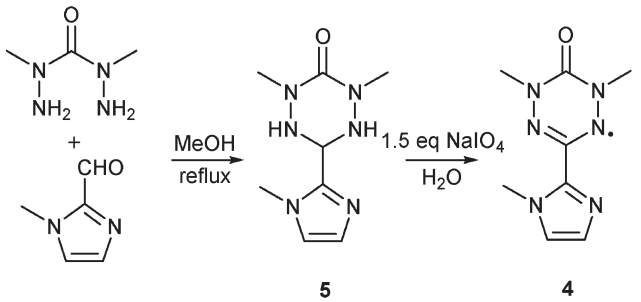

Scheme 1

graphite-monochromatized Mo-Kα radiation (λ = 0.71073 Å). The crystal structures were solved by direct methods (SHELXS-86).

CCDC reference numbers 601280–601283 (for **3**, **6**, **7**, and **9**). For crystallographic data in CIF or other electronic format see DOI: 10.1039/b603624d

Magnetic measurements

Variable-temperature magnetic data (2–300 K) were obtained with a Quantum Design MPMSXL SQUID magnetometer operating at field strengths of 1 and 3 T. All temperature-independent magnetic effects (diamagnetic and paramagnetic corrections) were corrected based on the slope of the linear regime of the *uncorrected* χT *vs.* T plots (with the exception of compound **6** where no such linear regime exists; in this instance Pascal's constants were used).

Results and discussion

Syntheses

Verdazyl radicals **2** and **3** were prepared according to literature methods. Verdazyl radical **4** was synthesized as shown in Scheme 1. Condensation of 1-methyl-2-imidazole carboxaldehyde with carbonic acid bis(1-methylhydrazide) afforded tetrazane **5**. Oxidation of the tetrazane with sodium periodate gave radical **4** as a deep orange powder.

Cu(II) complexes **6–9** were prepared from various combinations of verdazyls **2–4** with either $CuCl_2{\cdot}2H_2O$ or $Cu(hfac)_2{\cdot}2H_2O$ (Scheme 2). Crystalline or microcrystalline materials were obtained in good yield in all four cases, though single crystals of **8** were not of sufficient quality for structure determination. The infrared spectra of the copper complexes show the characteristic shift in the verdazyl ν(CO) value some 10–20 cm^{-1} higher than the corresponding spectra of the free (non-coordinated) radicals. Attempts to obtain EPR spectra of the complexes did not produce useful spectra; very weak signals corresponding to *non-coordinated* radicals (present as a minor impurity) were typically obtained.

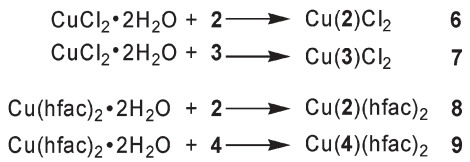

Scheme 2

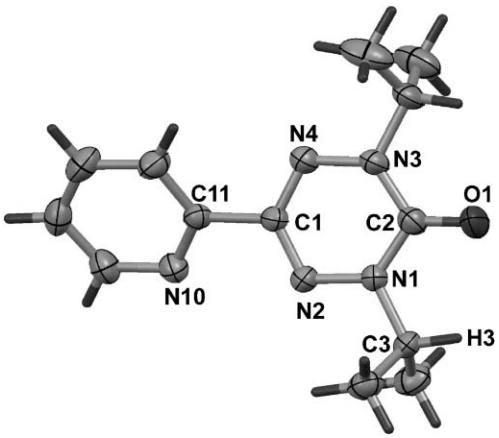

Fig. 1 Molecular structure of **3**. Selected bond lengths: O–C2 1.216(2), N1–N2 1.365(2), N1–C2 1.373(2), N2–C1 1.324(2), N3–N4 1.365(2), N3–C2 1.374(3), N4–C1 1.322(2), C1–C111.488(3) Å. Selected bond angles: N2–N1–C2 124.62(16), N1–N2–C1 114.33(15), N4–N3–C2 123.99(16), N3–N4–C1 114.95(16), N2–C1–N4 127.81(18), N1–C2–N3 114.30(18)°.

X-Ray structures

The *N*,*N*′-bis(isopropyl)-3-(2-pyridyl) verdazyl **3** was reported by Brook *et al.*[8] as one member of a general class of bis(isopropyl) substituted verdazyls which are significantly more stable than their *N*,*N*′-dimethyl analogues. However, no structures of these isopropyl-substituted verdazyls were reported. An ORTEP view of **3** is shown in Fig. 1. The internal structural features of the verdazyl ring are consistent with other structurally characterized 6-oxoverdazyls.[10] Both isopropyl substituents are oriented such that the C2–N1–C3–H3 torsion angle is only 1.2°, *i.e.* the methine proton H3 and the carbonyl oxygen are effectively *syn* with respect to one another. The N3 isopropyl group adopts an analogous conformation. There is a substantial torsion angle (26.8°) between the verdazyl and pyridine rings, in contrast to the *N*,*N*′-dimethyl-3-(2-pyridyl) verdazyl in which the pyridine and verdazyl rings are coplanar.[10c]

The solid state packing of **3** (Fig. 2) consists of one-dimensional slipped stacks parallel to *a* in which the verdazyl ring of one molecule is (partially) superimposed over the pyridine ring of a neighboring molecule within the stacks. There are several intermolecular contact distances within the stacks ranging from 3.6–3.9 Å, *i.e.* slightly longer than the van der Waals contact distance (~3.35 Å) for π-stacked rings. There are no appreciable intermolecular contacts between the slipped stacks.

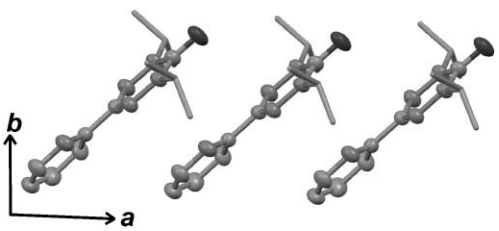

Fig. 2 Slipped stacks of radical **3**. Hydrogen atoms removed for clarity.

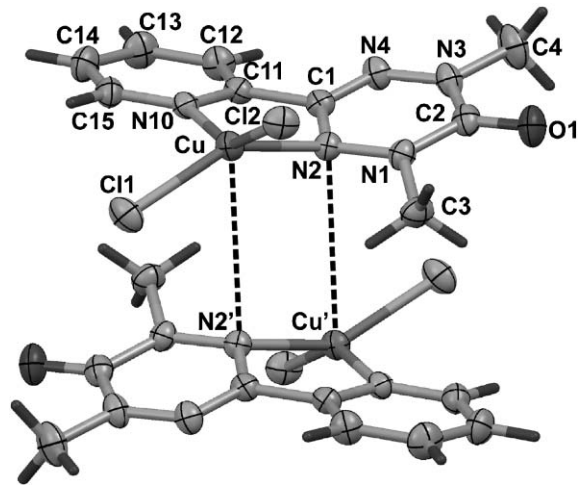

Fig. 3 Structure of the dimer of **6**. Selected bond lengths: Cu–Cl1 2.2234(5), Cu–Cl2 2.1965(5), Cu–N2 1.9992(14), Cu–N10 1.9921(15), O1–C2 1.210(2), N1–N2 1.349(2), N1–C2 1.385(2), N2–C1 1.358(2), N3–N4 1.342(2), N3–C2 1.379(3), N4–C1 1.306(2), Cu–N2′ 3.889 Å. Selected bond angles: Cl1–Cu–Cl2 102.02(2), N2–Cu–N10 81.34(6), N2–N1–C2 124.09(15), Cu–N2–C1 111.77(11), N1–N2–C1 114.34(14), N4–N3–C2 124.11(15), N3–N4–C1 115.90(15), Cu–N10–C11 114.56(12), N2–C1–N4 126.96(16)°.

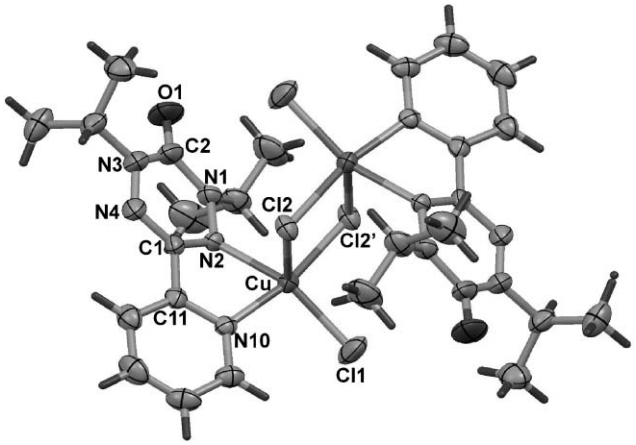

Fig. 4 Molecular structure of **7**. Only the major (55%) part of the disordered isopropyl group attached to N3 is shown (see Supporting Information for details). Selected bond lengths: Cu–Cl1 2.2136(13), Cu–Cl2 2.2140(11), Cu–Cl2′ 2.933(13), Cu–N2 2.058(3), Cu–N10 2.009(3), O1–C2 1.219(6), N1–N2 1.355(5), N1–C2 1.402(6), N2–C1 1.351(5), N3–N4 1.348(6), N3–C2 1.375(8), N4–C1 1.313(5) Å. Selected bond angles: Cl1–Cu–Cl2 96.46(5), Cl1–Cu–N10 95.27(10), Cl2–Cu–N2 94.63(9), Cl2–Cu–Cl2′ 86.42(9), N2–Cu–N10 78.98(13), N2–N1–C2 121.9(4), Cu–N2–N1 128.8(3), N1–N2–C1 115.2(3), N4–N3–C2 123.2(4), N3–N4–C1 115.4(4)°.

The molecular structure of copper complex **6**—an adduct of verdazyl **2** with $CuCl_2$—is depicted in Fig. 3. The verdazyl and pyridyl heterocyclic rings of ligand **2** are twisted by 19° with respect to each other. The copper ion lies in the plane of the pyridine ring but is 0.84 Å above the plane of the verdazyl ring. This leads to a non-planar environment at the coordinating verdazyl nitrogen (sum of angles at N2 = 350.5°). This contrasts the structures of other metal complexes of ligand **2** in which the ligand is essentially planar and the verdazyl donor nitrogen is flat. The C1–N4 (1.306 Å) and C1–N2 (1.358 Å) bonds are substantially different, in contrast to structures of uncoordinated verdazyls. This strong perturbation of radical structural metrics upon coordination is rare—the structures of verdazyl radicals coordinated to other metals show only minor structural changes.[4] Molecules of **6** weakly associate in the solid state to form the centrosymmetric dimeric structure containing long Cu–N contacts of 3.89 Å (slightly longer than the sum of the van der Waals distances for Cu and N at 3.87 Å). Taking the intermolecular Cu–N interactions into account, the overall geometry at the Cu is that of a highly distorted square pyramid: the " basal plane" is far from planar, as the $CuCl_2$ plane and the CuN_2 plane are twisted by 47.8° from one another and the axial coordination site is essentially a van der Waals contact.

The structure of the $CuCl_2$ complex of *N*,*N*′-diisoproyl verdazyl **3** (compound **7**) is also dimeric and consists of two molecules related by an inversion center, although the mode of association is more conventional in that it derives from chloride bridges (Fig. 4). The structural parameters within the monomeric units are quite similar to those found in **6**: the two rings of the verdazyl ligand are twisted by 21.5° with respect to each other, the Cu ion lies 1.11 Å out of the verdazyl plane, and there is substantial asymmetry in the C1–N2 and C1–N4 bond lengths. The isopropyl groups have reversed their orientation compared to that found in the structure of the free ligand: The methine hydrogens are now *anti* with respect to the C=O groups, presumably because this conformation is the least sterically congested at the metal center. Within the monomeric [Cu(**3**)Cl_2] unit, the copper ion is distorted square planar—the $CuCl_2$ and CuN_2 based planes intersect at an angle of 28°. The coordination sphere of the copper ion is completed by a long (2.933 Å) bridging interaction to Cl2 of a neighbouring molecule perpendicular to the "square plane" defined by the two chlorines and two nitrogens, leading to a distorted square pyramidal geometry. The two copper ions within the rectangular Cu_2Cl_2 core are 3.784 Å apart.

A view of the molecular structure of **9** is shown in Fig. 5. The verdazyl ligand **4** is essentially planar with a very small (4.8°) torsion angle between the imidazole and verdazyl rings. The geometry at the verdazyl N donor (N2) is also nearly planar (sum of angles = 359.4°). The bond lengths and angles within the verdazyl heterocycle are close to those of uncoordinated verdazyls, as well as other verdazyl complexes in which the structural effects of coordination appear to be minimal. The Cu(II) center is pseudo-octahedral, with a significant Jahn–Teller elongation evident from the very long axial bonds (Cu–N2 (2.544 Å) and Cu–O22 (2.234(2) Å)).

The solid state packing of **9** contains close intermolecular contacts between pairs of (coordinated) verdazyl rings of neighboring molecules (Fig. 6). The interplanar separation between the two rings is only 3.30 Å, and there are relatively close contacts involving the amide-like nitrogen atoms (N1–N3′ and N1′–N3, 3.389 Å).

Magnetic properties

The magnetic properties of verdazyl ligand **3** and the four copper complexes **6–9** were examined. The magnetic data and

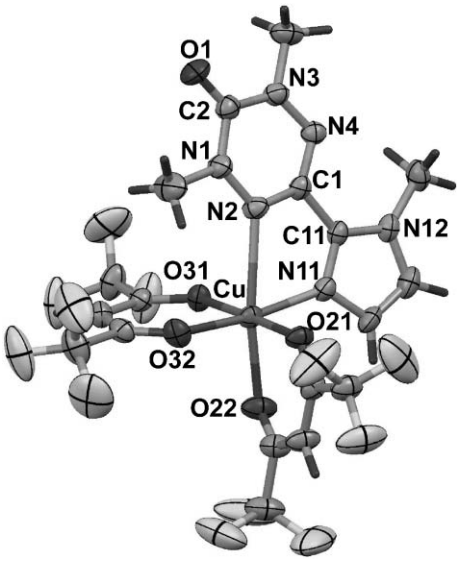

Fig. 5 Molecular structure of **9**. Selected bond lengths: Cu–O21 1.971(2), Cu–O22 2.234(2), Cu–O31 1.985(2), Cu–O32 1.948(2), Cu–N2 2.544(3), Cu–N11 1.961(3), N1–N2 1.361(4), N2–C1 1.327(4), N3–N4 1.359(4), N4–C1 1.328(4) Å. Selected bond angles: O21–Cu–O22 88.65(9), O31–Cu O32–91.04(9), N2–Cu–N11 71.92(10), N1–N2–C1 115.0(3), N3–N4–C1 114.0(3), Cu–N11–C11 124.1(2), N2–C1–N4 127.8(3)°.

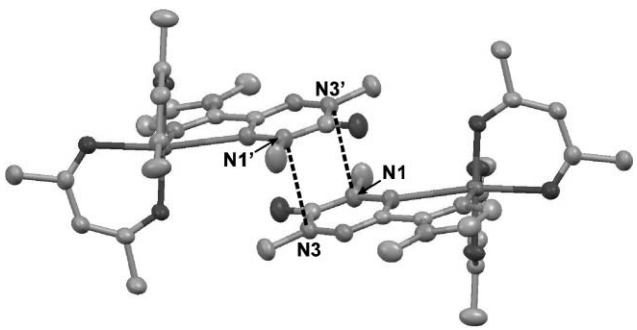

Fig. 6 Packing diagram for **9** with intermolecular verdazyl–verdazyl contact distances indicated (see text for details). Hydrogen and fluorine atoms removed for clarity.

model fit for radical **3** are shown in Fig. 7 in the form of a χ *vs.* T plot. The susceptibility rises with decreasing temperature and reaches a maximum value of 0.021 emu mol^{-1} at 6 K and then drops again below this temperature. The magnetic data were fit using a 1-dimensional antiferromagnetically coupled chain (Bonner–Fisher) model, in accord with the slipped stacked structure (Fig. 2) (see ESI‡ for details of all magnetic analyses). The best fit to the data was obtained with an intrachain interaction J of -3.3 cm^{-1}. The relatively weak intermolecular interactions are consistent with the molecular packing in **3**, in which there are no close radical–radical contacts to speak of.

The magnetic behaviour of complex **6** is presented in Fig. 8 as a χT *vs.* T plot. The room temperature χT value of 0.34 emu K mol^{-1} is much lower than the expected value for two noninteracting spins (χT = 0.750 emu K mol^{-1}), suggesting the presence of strong antiferromagnetic interactions.

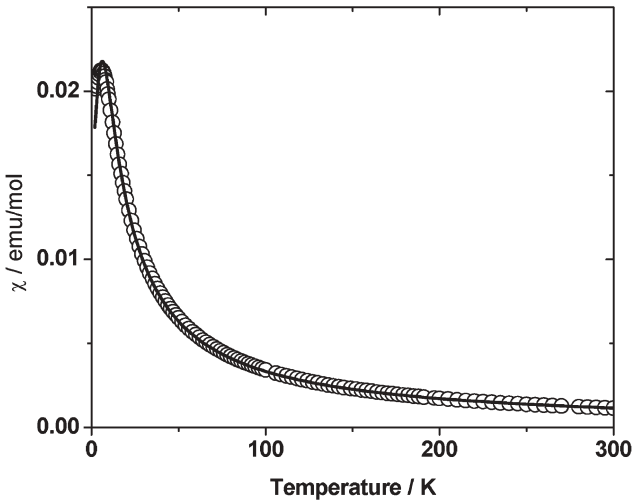

Fig. 7 Temperature dependence of χ for **3**. The solid line corresponds to the best fit to the data (see text).

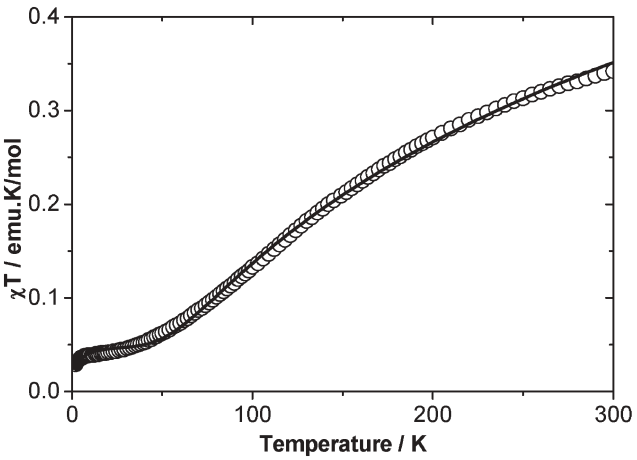

Fig. 8 χT *vs.* T plot for **6**. The solid line corresponds to the best fit to the data (see text).

As the temperature decreases, χT drops steadily down to very low temperatures. The magnetism was modelled using a modified Bleaney–Bowers equation in which a mean-field correction parameter was added to account for the possibility of copper–radical magnetic interactions between molecular units (*cf.* Fig. 3). Attempts to fit the data to a four-spin model (see below) failed. The best fit produced values for the intradimer interaction J_1 of -204 cm^{-1} and the mean field parameter, J_2 = -130 cm^{-1} (assuming z = 2; see ESI‡) as an estimate for the intermolecular copper–verdazyl interaction. A Curie–Weiss impurity of 3.1% was also included to adequately model the low-temperature data. The strong *intramolecular* antiferromagnetic copper–verdazyl exchange is consistent with several Cu(II) complexes of nitroxide radicals, in which equatorially bound nitroxides lead to strong antiferromagnetic coupling.[11] The *intermolecular* copper–verdazyl exchange (embodied by the mean-field adjustment to the model, see above) is also antiferromagnetic and fairly strong. The intermolecular Cu–verdazyl interaction can be regarded as occupying an axial site of the Cu coordination sphere, which

would seem to contrast the preference for weak ferromagnetic interactions between Cu(II) and axially coordinated nitroxides.[11] In most metal–radical complexes the radical–metal bonding interaction involves a lone pair on the radical donor atom, and the ligand-based spin resides in a different (often orthogonal) orbital. In complex **6**, however, the orientation of the axial Cu–N interaction is such that the p-lobe on the nitrogen which interacts with the metal is part of the radical SOMO itself.

Complex **7** $(Cu(\mathbf{3})Cl_2)_2$ is diamagnetic at room temperature and remains so down to 40 K, at which point a paramagnetic impurity gives rise to a weak paramagnetic signal. Magnetostructural correlations on a wide variety of dinuclear Cu(II) complexes bridged by chlorides have led to empirical relationships between the exchange interaction involving the copper-based spins and structural parameters associated with the Cu_2Cl_2 core, specifically the ratio θ/r, where θ represents the Cu–Cl–Cu angle and r is the longer of the two CuCl bonds.[12] For compound **7** this ratio is 31.9° $Å^{-1}$ which, when compared to the small library of dinuclear chloro-bridged copper complexes,[12] leads to the prediction that the Cu–Cu exchange interaction should be near zero or very weakly antiferromagnetic. The diamagnetism in **7** must therefore arise from extremely strong antiferromagnetic copper–verdazyl magnetic interactions. This is again consistent with the precedent offered by copper(II)-nitroxide complexes.[11]

The χT *vs.* T plot for complex **9** is shown in Fig. 9. Above 100 K χT is nearly constant with a value (0.81 emu K mol^{-1}) slightly higher than the expected value for two non-interacting spins (0.75 emu K mol^{-1}). Below 100 K, χT drops and plateaus at $\sim$20 K to a value of $\sim$0.5 emu K mol^{-1} before decreasing again at the lowest attainable temperatures. In light of the close approach of pairs of molecules so as to produce short radical–radical contacts (Fig. 6) the magnetism of this complex was modelled as a *four*-spin system consisting of an *inter*molecular $J_{rad-rad}$ and an *intra*molecular J_{Cu-rad}. The quantitative fit does not appear (Fig. 9) to be particularly good visually, although the fit reproduces the gross temperature dependence of χT and a reasonable goodness of fit was

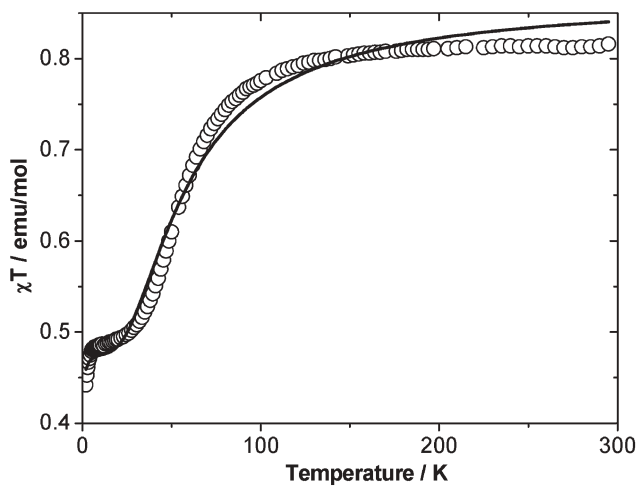

Fig. 9 χT *vs.* T plot for **9**. The solid line corresponds to the best fit to the data (see text).

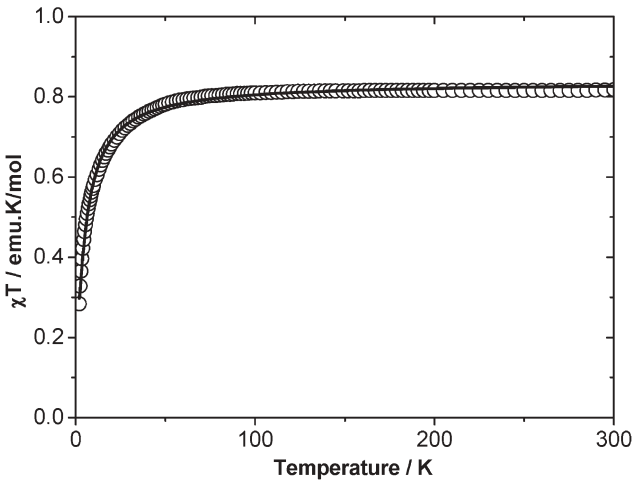

Fig. 10 χT *vs.* T plot for **8**. The solid line corresponds to the best fit to the data (see text).

obtained ($R = 5 \times 10^{-4}$). From the model we obtain $J_{rad-rad} = -39.5$ cm^{-1}, $J_{Cu-rad} = +6$ cm^{-1} and a Weiss constant $\theta = +0.6$ K (associated with a paramagnetic impurity present in $\sim$0.9%) and the mean g-value was fixed at 2.1 to reproduce the high-temperature (plateau) value. Thus, the copper–radical magnetic exchange is ferromagnetic, albeit very weakly so, while the specific intermolecular magnetic coupling between π-stacked radicals is more substantial and antiferromagnetic. The Cu(II)–verdazyl ferromagnetism is consistent with axially coordinated Cu(II) nitroxide complexes and with the orbital symmetry arguments that dictate the conditions for ferromagnetic exchange in metal–radical systems in general.[13]

Although no crystal structure of the other hfac-based copper–verdazyl complex **8** was obtained, spectroscopic and analytical data are consistent with it possessing a molecular structure similar to that of **9**. A χT *vs.* T plot for **8** is presented in Fig. 10. Above 100 K the value of χT is constant at about 0.81 emu K mol^{-1}, the same as the high temperature value for compound **9**. Below 100 K the χT product drops smoothly and does *not* plateau as was seen in **9**. The data was fit with a Bleaney–Bowers based model, modified with a mean-field parameter and a small proportion of a Curie–Weiss impurity. The optimum fit yielded $g = 2.1$ (fixed; *vide infra*) $J_{Cu-rad} = +5$ cm^{-1}, $J_{inter} = -2$ cm^{-1} (assuming $z = 2$ in the mean field parameter). The CW impurity fraction was 1.2% with a Weiss constant $\theta = +1.5$ K. Thus the intramolecular copper–radical coupling is again weakly ferromagnetic. We interpret differences in the low temperature magnetism between **8** and **9** as arising from different packing patterns in the solid state—the lack of plateau in the former suggest that the coordinated verdazyls do not adopt a packing mode analogous to that observed in **9**.

Summary

We have described the synthesis, structures, and magnetic properties of several Cu(II) complexes of verdazyl radicals. In general, the qualitative magnetostructural correlations developed for nitroxide–copper(II) complexes hold for verdazyl complexes as well: equatorially bound radicals are

strongly antiferromagnetically coupled (compounds **6** and **7**) whereas axially coordinated radicals are ferromagnetically coupled (compounds **8** and **9**) but only very weakly so due to the Jahn–Teller distortion which significantly lengthens the Cu–vd bonds.

Acknowledgements

We thank the University of Victoria and the Natural Sciences and Engineering Research Council of Canada for financial support. We also thank Dr Natia L. Frank for the use of her SQUID magnetometer and helpful discussions.

References

1 A. Caneschi, D. Gatteschi, R. Sessoli and P. Rey, *Acc. Chem. Res.*, 1989, **22**, 392–398.
2 (*a*) M. Manriquez, G. T. Yee, S. MacLean, A. J. Epstein and J. S. Miller, *Science*, 1991, **252**, 1415–1417; (*b*) J. P. Fitzgerald, B. B. Kaul and G. T. Yee, *Chem. Commun.*, 2000, 49–50; (*c*) R. Clerac, S. O'Kane, J. Cowen, X. Ouyang, R. Heintz, H. H. Zhao, M. J. Bazile and K. R. Dunbar, *Chem. Mater.*, 2003, **15**, 1740–1850; (*d*) E. B. Vickers, T. B. Selby and J. S. Miller, *J. Am. Chem. Soc.*, 2004, **126**, 3716–17.
3 (*a*) K. Inoue, T. Hayamizu, H. Iwamura, D. Hashizume and Y. Ohashi, *J. Am. Chem. Soc.*, 1996, **118**, 1803–1804; (*b*) H. O. Stumpf, L. Ouahab, Y. Pei, D. Grandjean and O. Kahn, *Science*, 1993, **261**, 447–449.
4 (*a*) R. G. Hicks, M. T. Lemaire, L. K. Thompson and T. M. Barclay, *J. Am. Chem. Soc.*, 2000, **122**, 8077–8078; (*b*) T. M. Barclay, R. G. Hicks, M. T. Lemaire and L. K. Thompson, *Chem. Commun.*, 2000, 2141–2142; (*c*) T. M. Barclay, R. G. Hicks, M. T. Lemaire and L. K. Thompson, *Inorg. Chem.*, 2001, **40**, 6521–6524; (*d*) T. M. Barclay, R. G. Hicks, M. T. Lemaire and L. K. Thompson, *Inorg. Chem.*, 2001, **40**, 5581–5584; (*e*) T. M. Barclay, R. G. Hicks, M. T. Lemaire, L. K. Thompson and Z. Q. Xu, *Chem. Commun.*, 2002, 1688–1689; (*f*) T. M. Barclay, R. G. Hicks, M. T. Lemaire and L. K. Thompson, *Inorg. Chem.*, 2003, **42**, 2261–2267; (*g*) R. G. Hicks, B. D. Koivisto and M. T. Lemaire, *Org. Lett.*, 2004, **6**, 1887–1890; (*h*) M. T. Lemaire, T. M. Barclay, L. K. Thompson and R. G. Hicks, *Inorg. Chim. Acta*, 2006, in press.
5 (*a*) D. J. R. Brook, V. Lynch, B. Conklin and M. A. Fox, *J. Am. Chem. Soc.*, 1997, **119**, 5155–5162; (*b*) D. J. R. Brook, S. Fornell, B. Noll, G. T. Yee and T. H. Koch, *J. Chem. Soc., Dalton Trans.*, 2000, 2019–2022; (*c*) D. J. R. Brook, S. Fornell, J. E. Stevens, B. Noll, T. H. Koch and W. Eisfeld, *Inorg. Chem.*, 2000, **39**, 562–567; (*d*) D. J. R. Brook and V. Abeyta, *J. Chem. Soc., Dalton Trans.*, 2002, 4219–4223.
6 J. Z. Wu, E. Bouwman, J. Reedijk, A. M. Mills and A. L. Spek, *Inorg. Chim. Acta*, 2003, **351**, 326–330.
7 C. L. Barr, P. A. Chase, R. G. Hicks, M. T. Lemaire and C. L. Stevens, *J. Org. Chem.*, 1999, **64**, 8893–8897.
8 E. C. Pare, D. J. R. Brook, A. Brieger, M. Badik and M. Schinke, *Org. Biomol. Chem.*, 2005, **3**, 4258–4261.
9 R. J. Casey and W. R. Walker, *J. Inorg. Nucl. Chem.*, 1967, **29**, 1301.
10 (*a*) D. J. R. Brook, H. H. Fox, V. Lynch and M. A. Fox, *J. Phys. Chem.*, 1996, **100**, 2066–2071; (*b*) F. A. Neugebauer, H. Fischer and C. Krieger, *J. Chem. Soc., Perkin Trans. 2*, 1993, 535–544; (*c*) R. G. Hicks, M. T. Lemaire, L. Ohrstrom, J. F. Richardson, L. K. Thompson and Z. Q. Xu, *J. Am. Chem. Soc.*, 2001, **123**, 7154–7159.
11 A. Caneschi, D. Gatteschi and P. Rey, *Prog. Inorg. Chem.*, 1991, **39**, 331–429.
12 (*a*) W. E. Marsh, K. C. Patel, W. E. Hatfield and D. J. Hodgson, *Inorg. Chem.*, 1983, **22**, 511–515; (*b*) W. A. Alves, R. H. de Almeida Santos, A. Paduan-Filho, C. C. Becerra, A. C. Borin and A. M. da Costa Ferreira, *Inorg. Chim. Acta*, 2004, **357**, 2269–2278.
13 R. G. Hicks, *Aust. J. Chem.*, 2001, **54**, 597–600 and references cited therein.

